Manipulation of extinction spectra of P3HT/PMMA medium arrays on silicon substrate containing self-assembled gold nanoparticles

Ming-Chung Wu [a], Shih-Wen Chen [b], Jia-Han Li [b], Yi Chou [c], Jhih-Fong Lin [c], Yang-Fang Chen [d], Wei-Fang Su [c,*]

[a] Department of Chemical and Materials Engineering, Chang Gung University, Taoyuan 333-02, Taiwan
[b] Department of Engineering Science and Ocean Engineering, National Taiwan University, Taipei 106-17, Taiwan
[c] Department of Materials Science and Engineering, National Taiwan University, Taipei 106-17, Taiwan
[d] Department of Physics, National Taiwan University, Taipei 106-17, Taiwan

HIGHLIGHTS

► We can tune the extinction spectra of P3HT/PMMA by manipulating the medium arrays.
► These optical behaviors of P3HT/PMMA medium arrays are well described by FDTD simulation results.
► Adding the Au nanoparticles can give more functionalities for sensing applications.

GRAPHICAL ABSTRACT
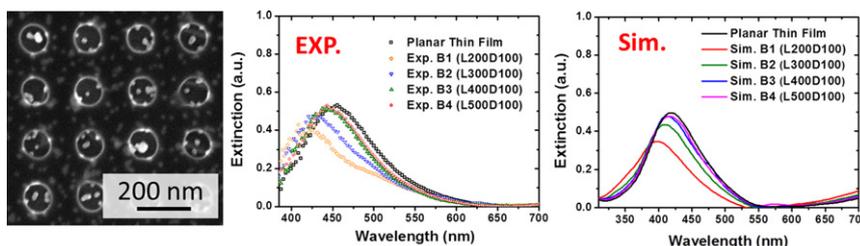
ABSTRACT

In this study, we report a simple novel approach to modulate the extinction spectra of P3HT/PMMA by manipulating the medium arrays on a substrate that is coated with self-assembled gold nanoparticles. The 20 nm gold nanoparticles were synthesized and then self-assembled on the APTMS/silicon substrate surface by immersing the substrate into the gold colloid suspension. A high-resolution P3HT/PMMA photoluminescent electron beam resist was used to fabricate various square hole arrays on the substrate containing gold nanoparticles. The P3HT/PMMA medium composition causes the blue shifts in the extinction peaks of up to 40.6 nm by decreasing the period from 500 nm to 200 nm for P3HT/PMMA square hole arrays with a diameter of 100 nm. The magnitude of blue shift is directly proportional to the product of the changes of medium refractive index and the array structure factor. These peak shifts and intensity of extinction spectra for various P3HT/PMMA medium arrays are well described by the finite-difference time-domain (FDTD) simulation results. Since this simple cost-effective technique can tune the extinction spectrum of medium and adding the gold nanoparticles can give more functionalities for sensing applications, such as surface-enhanced Raman scattering (SERS), that provides good opportunities for the design and fabrication of new optoelectronic devices and sensors.

1. Introduction

Modulating optical properties of polymer array structure has recently took attentions in a wide range of applications, for

example, control of the cell grow direction [1], the transmission enhancement on waveguides [2,3], the light trapping increase in photovoltaic cells [4] and tunable resonance frequency of sensors assisted by surface plasmon resonance (SPR) [5,6]. Using the periodic patterns is one popular method to control the field enhancements in the polymer structures. These kind of patterns can be easily fabricated by the lithography techniques such as

* Corresponding author.
E-mail address: suwf@ntu.edu.tw (W.-F. Su).

a

b

c

d

e

P3HT:PMMA
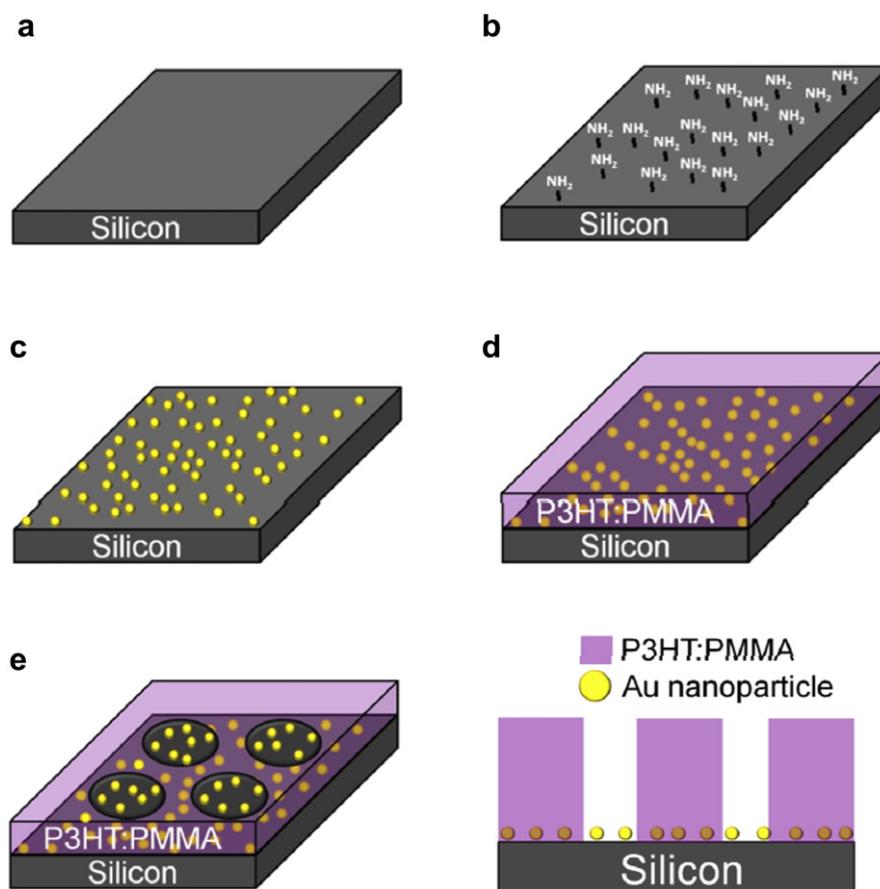
Au nanoparticle

Fig. 1. Fabricating processes of the P3HT/PMMA medium arrays on self-assembled gold nanoparticles coated silicon substrate. (a) Clean silicon wafer by acid washing, (b) immerse silicon wafer in APTMS solution, (c) immerse APTMS coated silicon wafer in gold nanoparticles solution to form self-assembled gold nanoparticles on the substrate, (d) spin coat P3HT/PMMA electron beam resist on the self-assembled gold nanoparticles coated silicon substrate, and (e) obtain P3HT/PMMA medium arrays on self-assembled gold nanoparticles coated silicon substrate by electron beam lithography and its cross-section view.

photolithography [7], colloidal lithography [8], and electron beam lithography [9]. The thermal evaporation can be used to deposit the noble metals on the structures for more functionalities for detecting and sensing applications. For example, the enhancements in the overall fluorescence efficiency and surface-enhanced Raman scattering (SERS) in proximity to the surface plasmon polaritons of structured noble metal substrates have been studied [10–12]. Also, it gives more sensitivities for the metallic structures with localized surface plasmon resonance (LSPR) [13,14], which is strongly dependent on the size [15,16], shape [17], surrounding environment [18,19], metal characteristics [20], and metal thickness [21]. While interesting, the noble metal thermal evaporation method is a costly vacuum process and it results the metal waste in the vacuum chamber. Using noble metal nanoparticles for controlling the field enhancements has attracted a lot of interest due to the material cost reduction and it gives strong local electromagnetic fields in the structures [22,23]. Recent studies show that the field enhancements of a nanoparticle array is related to the medium refractive index [5,6,24–27]. Van Duyne's group reported the plasmon band shift resulting from a local medium refractive index change which was caused by binding specific molecule to ligand-modified nanoparticles surface [28], and observed short-range distance dependence for nanoscale optical biosensor [29]. M. Käll's group immersed a substrate containing gold hole arrays in various media with different refractive indices (n), such as dry nitrogen ($n = 1$), water ($n = 1.333$), and p-xylene ($n = 1.496$), and found the significant red shift with increasing n [19]. El-Sayed's group reported a linear increased surface plasmon resonance shift

produced from the electromagnetic coupling between the noble metal nanoparticles with increasing the dielectric constant of the medium by using both a quasi-static model and discrete dipole approximation simulations [30]. Moreover, the useful applications in consideration of mass production in industry require the capability to tune the optical properties using a simple process with lower material cost.

Here, we can achieve this by manipulating P3HT/PMMA medium arrays to modulate the degree of coupling between P3HT/PMMA extinction spectra and field enhancements of gold nanoparticles. The P3HT/PMMA medium is made by blending P3HT and PMMA with 1:1000 ratio. The SPR is fixed using self-assembled gold nanoparticles on 3-aminopropyltrimethoxysilane coated silicon substrate (APTMS/Si). The tunability of extinction spectra can be obtained by fabrication of several P3HT/PMMA arrays with different structures on this kind of fixed SPR substrate, so the extinction spectra can be varied by the coupling between P3HT/PMMA absorption and gold nanoparticles surface plasmon resonance. In addition, the dependence of the extinction spectra on the changes of P3HT/PMMA medium arrays is also shown by theoretical prediction using finite-difference time-domain (FDTD) simulation method.

2. Experimental section and simulation setup

All chemicals were purchased and used as received without further purification. The 20 nm gold nanoparticles were synthesized with some modification according to literatures [31–33]. To
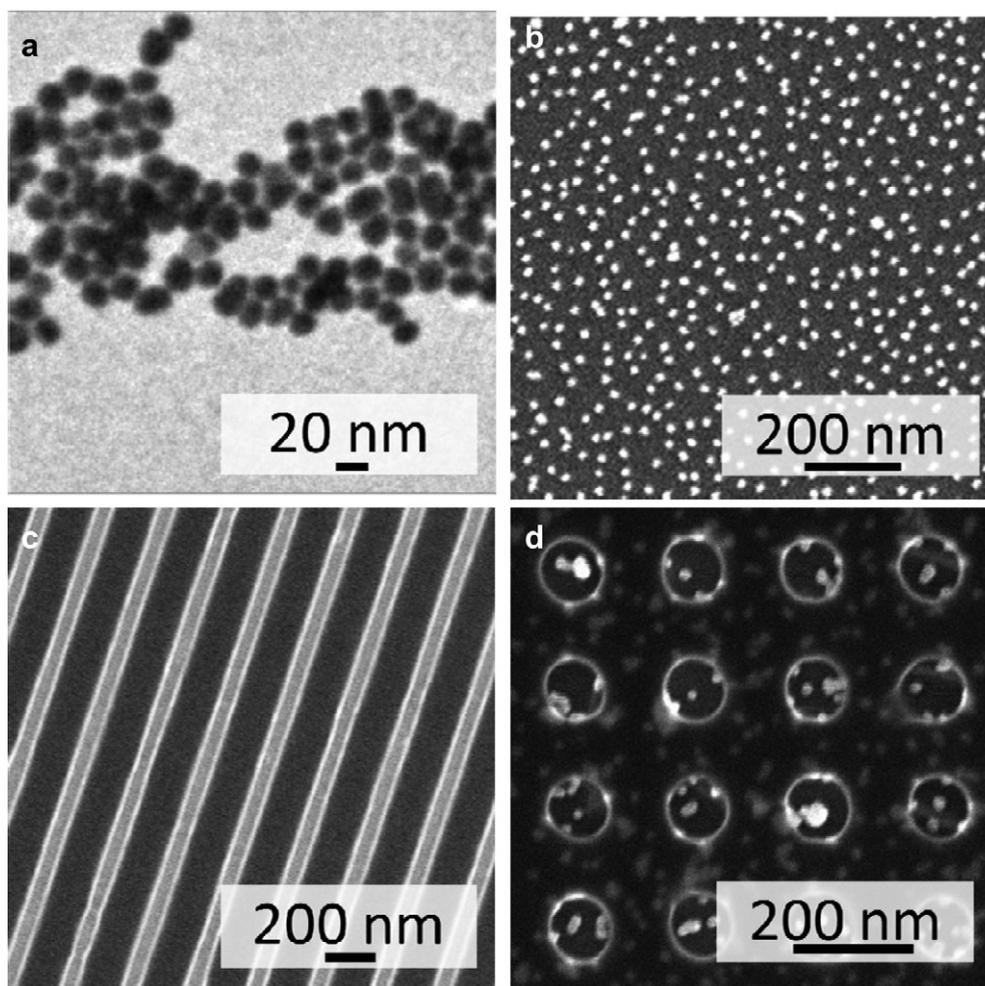
Fig. 2. (a) TEM image of gold nanoparticles, (b) SEM image of gold nanoparticles self-assembled onto the surface of APTMS/Si substrate. (c) SEM image of the periodic lines with a width of 90 nm and an interval of 300 nm made from 0.1 wt% P3HT/PMMA resist, and (d) SEM image of P3HT/PMMA medium square hole array with a period of 200 nm and a diameter of 100 nm on the self-assembled gold nanoparticles coated APTMS/Si substrate.

obtain self-assembled gold nanoparticles on APTMS/Si substrates, 30 mg of gold(III) chloride trihydrate (HAuCl$_4$. 3H$_2$O, Acros, 99.8%) was dissolved in 15.0 g deionized water and heated to 100 °C while stirring vigorously. 10 mg of trisodium citrate dihydrate (C$_6$H$_5$Na$_3$O$_7$. 2H$_2$O, Acros, 99%) in 0.8 ml deionized water was then added and kept at 100 °C for 5 min. The reaction was cooled to room temperature and then diluted by deionized water to make a final product of 0.01 wt% gold colloid solution. The cleaned silicon substrates were immersed in a solution of 3-aminopropyltrimethoxysilane (APTMS, Acros, 97%)/deionized water/isopropyl alcohol with a volume ratio of (1:1:40 v/v) for 24 h. After the immersion, the sample was cleaned by deionized water and baked at 120 °C for 2 h. The gold nanoparticles were self-assembled on the APTMS/Si substrate surface by immersing the substrate into the gold colloid suspension for 12 h. The substrate was rinsed with deionized water immediately after removing from gold colloid suspension, and was dried in the oven at 120 °C for 2 h.

The regioregular poly(3-hexylthiophene) (P3HT) with MW ∼13,500 Da were synthesized according to the literature [34]. The 0.2 wt% P3HT and 2.0 wt% PMMA (Aldrich, MW ∼996,000) polymer solutions were prepared in chlorobenzene and stirred for 2 h and 48 h at room temperature, respectively. Then, the photoluminescent e-beam resist (P3HT/PMMA) was prepared by mixing both polymer solutions under stirring for 24 h at room

temperature. The resist was spin coated onto silicon wafers at 3000 rpm for 90 s to give a nominal thickness of ∼200 nm. Finally, the P3HT/PMMA thin films were baked at 180 °C for 10 min. High-resolution nanolithography was performed by writing specific patterns across a 150 μm field with a 2.5 nm beam step size using an Elionix ELS-7000EX high-resolution electron beam lithography system. The system provides a stable 1.8 nm electron beam using high beam currents at 100 keV. After the film was exposed to the electron beam, it was developed by using mixed solvents of methyl isobutyl ketone and isopropanol (25:75 by volume) for 40 s, then isopropanol for 20 s and finally, deionized water for 20 s. These processes are illustrated in Fig. 1. Field-emission scanning electron microscopy (FE-SEM, Elionix ERA-8800FE, Japan) was used to observe the microstructures of P3HT/PMMA arrays on silicon substrate and P3HT/PMMA arrays on self-assembled gold nanoparticles coated silicon substrate. The extinction spectra of P3HT/PMMA arrays on self-assembled gold nanoparticles coated silicon substrate were evaluated using a spectral microreflectometer (Mission Peak Optics, MP100-ME) equipped with an optical microscope. Unpolarized light was focused on the P3HT/PMMA array under the silicon substrate at a spot size <20 μm to measure the difference between the incident and reflected light with wavelengths ranging from 365 nm to 850 nm.
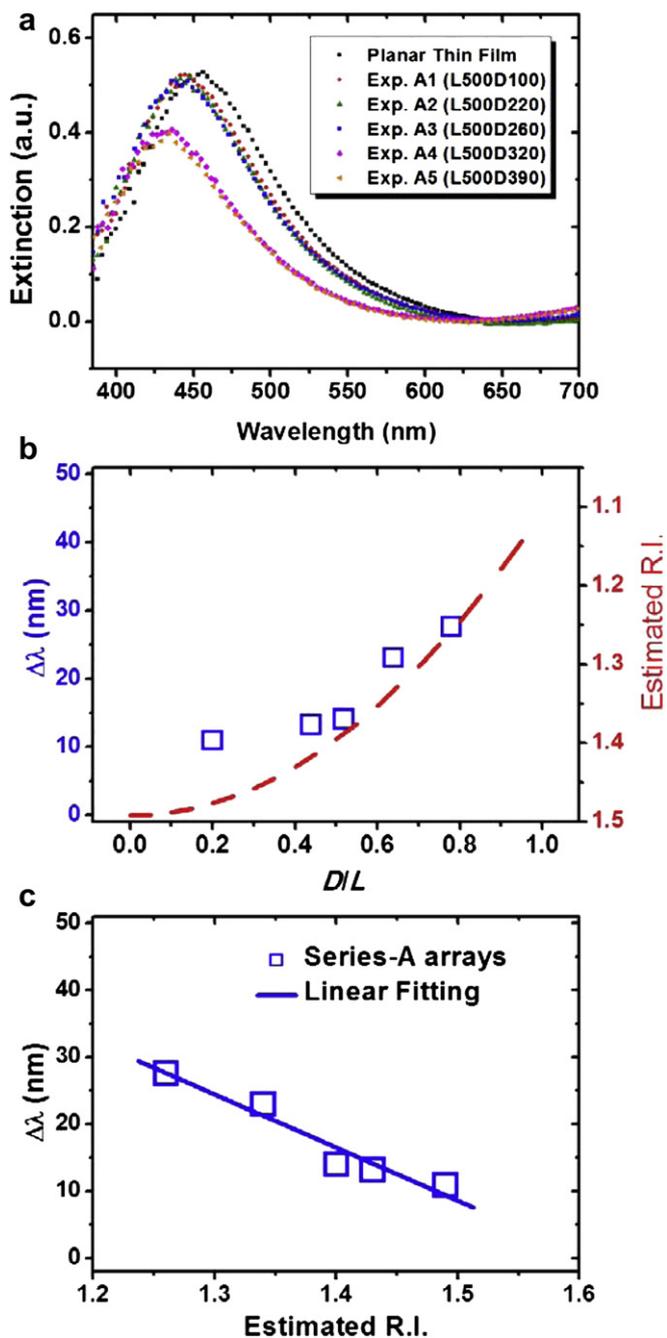
Fig. 3. (a) The extinction spectra of Series-A P3HT/PMMA medium arrays on self-assembled gold nanoparticles coated APTMS/Si substrate, (b) the relationship between the blue shift of extinction peak ($\Delta\lambda_{blue-shift} = |\lambda_{max} - \lambda_0|$.) and the spacing ratio (D_{hole}/L) of array and the red dotted line is the estimated refractive index of P3HT:PMMA medium with different array spacing ratio, and (c) a linear relationship between $\Delta\lambda_{blue-shift}$ and the estimated refractive index. [For interpretation of the references to colour in this figure legend, the reader is referred to the web version of this article.]

To simulate the extinction spectra of P3HT/PMMA medium arrays on the self-assembled gold nanoparticles coated silicon substrate, we used a commercial software (Lumerical FDTD Solutions Release 6.5) based on the finite-difference time-domain method (FDTD), which can solve Maxwell's Equation for complex geometries efficiently. For the simulation parameters, we chose the diameter of gold nanoparticles to be 20 nm mirroring our bench experiments. The optical properties of gold are obtained from the
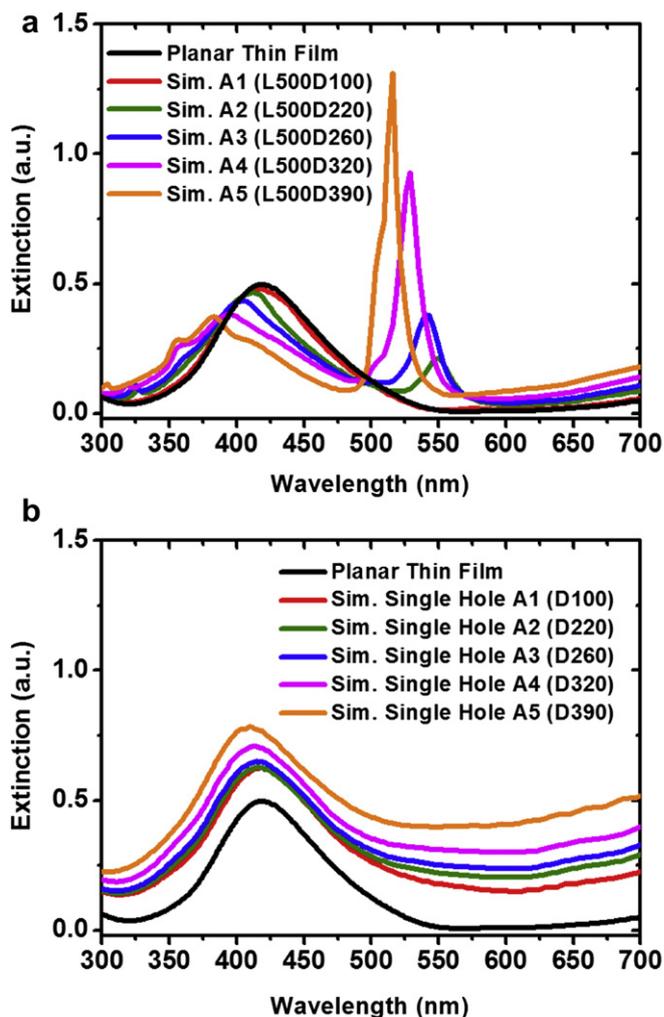
Fig. 4. Simulated extinction spectra of (a) Series-A arrays of 500 nm lattice constant with different hole diameters (100, 220, 260, 320 and 390 nm) and (b) single hole with different hole diameters (100, 220, 260, 320 and 390 nm) on self-assembled gold nanoparticles coated silicon substrate by FDTD method.

experimental data by Johnson and Christy [35]. The refractive indexes of silicon substrates at different wavelengths are adopted from Palik's handbook [36]. The P3HT/PMMA (1:1000 blending ratio) medium thickness is 200 nm and its refractive index was estimated by taking the value of 1.503 from Kasarova's study [37].

3. Results and discussion

Although the average particle size of synthesized gold nanoparticles is ∼20 nm as shown in Fig. 2(a), they tended to aggregate on the substrate. By tuning two fabrication parameters 1) immersion time and 2) concentration of gold nanoparticles solution, we can obtain high-quality isolated gold nanoparticles on APTMS/Si substrate for surface plasmon coupling study as shown in Fig. 2(b). We have synthesized P3HT/PMMA electron beam resists in our laboratory that exhibit high-resolution patternable property and are useful in the applications of optoelectronic devices [38]. The resist made from 0.1 wt% P3HT in P3HT/PMMA blend exhibits a line width roughness of ∼4.2 nm, which is close to that of the commercial PMMA electron beam resist (4.1 nm). The periodic line patterns fabricated from this resist has a width of 90 nm and an interval of 300 nm as shown in Fig. 2(c). This resist was selected for
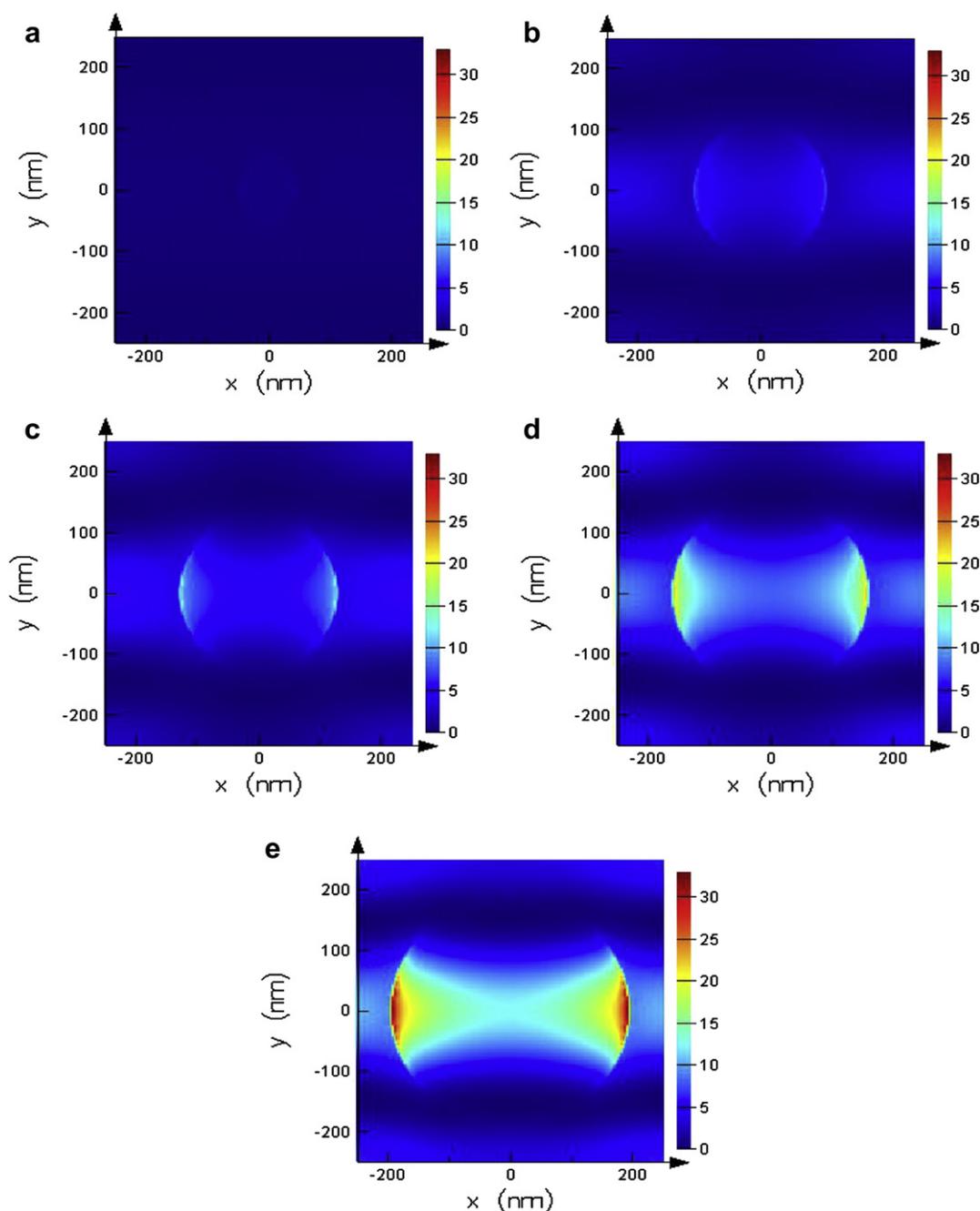
Fig. 5. Electric field distribution at the second peak maximum wavelength on the surface of the Series-A arrays with different hole diameters (a) 100 nm, (b) 220 nm, (c) 260 nm, (d) 320 nm and (e) 390 nm, on self-assembled gold nanoparticles coated silicon substrate as shown in Fig. 4(a) by FDTD method.

use as the medium to be lay on the top of self-assembled gold nanoparticles coated silicon substrate for coupling the surface plasmon resonance. Fig. 2(d) shows the SEM images of patterned P3HT/PMMA layer on self-assembled gold nanoparticles coated silicon substrate, where individual gold nanoparticles can be observed clearly. The results confirm that various patterns can be easily fabricated using the P3HT/PMMA electron beam resist and the gold nanoparticles remain on the substrate following the developing procedure.

Next, we designed two series of P3HT/PMMA square hole arrays to study the medium effect on the coupling between P3HT/PMMA extinction properties and the gold nanoparticles SPR. The sample size of various P3HT/PMMA square hole arrays was about

$40 \times 40 \ \mu m^2$. These arrays were fabricated on the same self-assembled gold nanoparticles coated APTMS/Si substrate to make sure that the effect of gold nanoparticle SPR on every array was similar. Series-A arrays had a fixed period of 500 nm with different diameter of holes that were ranged from 100, 220, 260, 320, to 390 nm. The extinction peak of P3HT/PMMA is 457.8 nm for its planar film on self-assembled gold nanoparticles coated silicon substrate. The extinction peak is mainly from the absorption characteristics of the P3HT/PMMA. In comparison of the simulations for the cases with and without gold nanoparticles, we found that the case with gold nanoparticles can enhance extinction peaks a little bit with slight blue shift. Changing the structural parameters of P3HT/PMMA square hole arrays can lead to the extinction peak
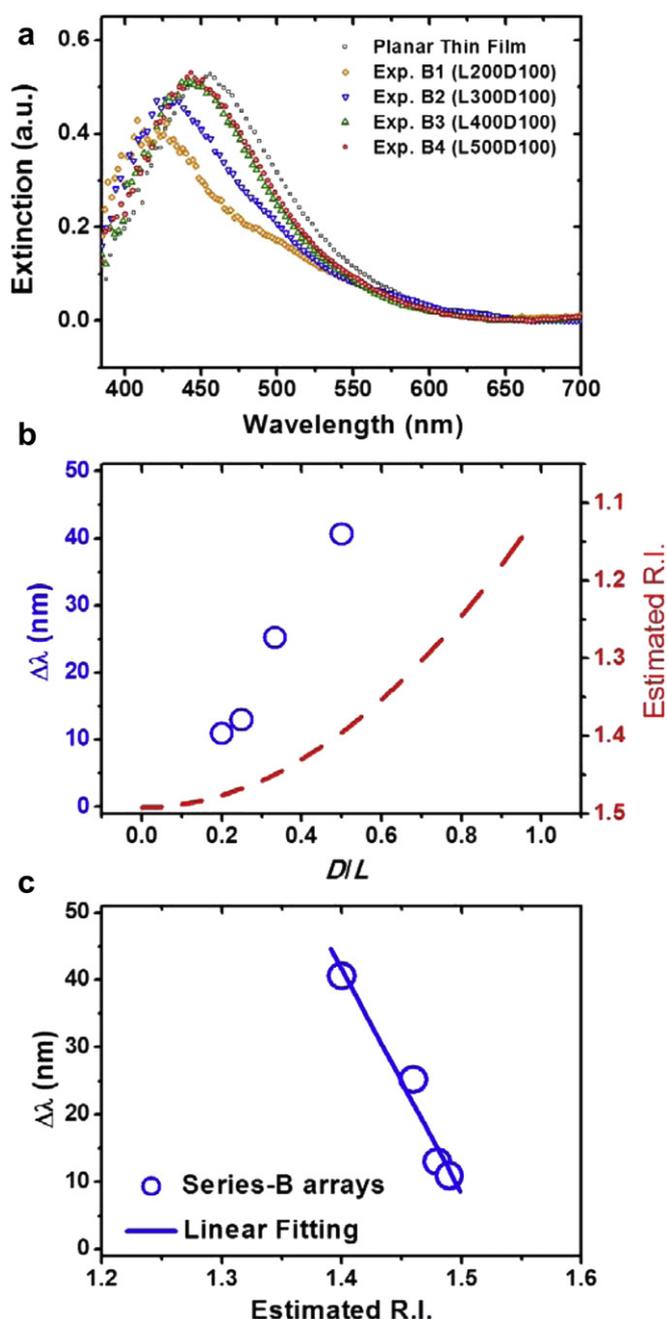
Fig. 6. (a) The extinction spectra of Series-B P3HT/PMMA medium arrays on self-assembled gold nanoparticles coated silicon substrate, (b) the relationship between D_{hole}/L and $\Delta\lambda_{blue-shift}$ and the red dotted line is the estimated refractive index of P3HT:PMMA medium with different array spacing ratio, and (c) a linear relationship between $\Delta\lambda_{blue-shift}$ and the estimated refractive index. [For interpretation of the references to colour in this figure legend, the reader is referred to the web version of this article.]

shift due to the different extent of coupling between P3HT/PMMA absorption and gold nanoparticles SPR. For Series-A arrays, the extinction spectra show blue shifts (the maximum $\Delta\lambda_{blue-shift}$ ~27.6 nm) when varying the hole diameter from 100 to 390 nm with a fixed period of 500 nm as shown in Fig. 3(a). The blue shift results from the decrease in the volume fraction or refractive index of medium. To quantitatively understand the observed results, we re-plotted the relationships between the array spacing ratio (D/L) and $\Delta\lambda_{blue-shift}$, and the red dotted line is the estimated refractive

index of P3HT/PMMA medium with different D/L. The refractive index of the planar thin film of P3HT/PMMA is about 1.503, and the refractive index of air is 1.000. Thus, the estimated refractive index of the P3HT/PMMA square hole array is in direct proportion to the volume fraction of P3HT/PMMA medium array and the estimated refractive index decreases with increasing hole area ratio (Fig. 3(b)). Moreover, we also re-plotted the blue shift of the extinction peak as a function of the estimated refractive index as shown in Fig. 3(c). The $\Delta\lambda_{blue-shift}$ increases with the decreasing of the estimated refractive index for Series-A arrays, and the relationship between $\Delta\lambda_{blue-shift}$ and the estimated refractive index shows a good linear fitting (blue solid line).

In addition, the simulated extinction spectra of various P3HT/PMMA arrays with periodic nanoparticles in square arrangement were also obtained by employing the FDTD method. The separation between nanoparticles is 50 nm. As compared to the experimental data, the simulation results of Series-A arrays show additional sharp extinction peaks that appear between 510 nm and 550 nm when the hole diameter is varied (Fig. 4(a)). In our experiments, Series-A arrays show extinction peaks at 430.2–446.9 nm (Fig. 3(a)) and the second peak was not observed. Subsequently, we tried to calculate the resonance modes for the second peaks of Series-A square hole arrays. The electric field distribution on the surface of Series-A square hole arrays at the second peak maximum wavelength was shown in Fig. 5. In addition, the electric field distribution of the first peak in Series-A arrays and Series-B arrays are shown in Figure S1 in Supporting Information. When the diameter of hole increases for Series-A square hole arrays, the electric field intensity becomes more concentrative around sidewall and affects the nearest hole. The smaller gap between two holes will result in the stronger intensity of coupled electric field. The simulation results also show the structure of hole arrays influences the extinction spectra. Then, we tried to figure out the cause of the second peak of Series-A in the simulation results. Fig. 4(b) shows the simulation results of the single hole with different hole diameters. The second sharp peaks are disappeared and only broad peaks at 400–450 nm are present. The peaks around 400–450 nm are resulted from the absorption of P3HT/PMMA (457.8 nm) which is coupled with the gold nanoparticles SPR. Because the sample size of P3HT/PMMA square hole arrays are about $40 \times 40\ \mu m^2$, this means that it is not infinite number of holes as simulated in Fig. 4(a). Also, the size and the shape of the holes may be not controlled perfectly in fabrication. Thus, the absence of second peaks around 510–550 nm in our experiments may be resulted from the unperfected periodic arrays of P3HT/PMMA square hole. Figure S2 shows the simulation results with variable diameter hole structures in Supporting Information. Besides, the random orientation of gold nanoparticles may affect the second peak.

Series-B arrays have a fixed hole diameter of 100 nm with different periods that are ranged from 200, 300, 400, to 500 nm. The extinction spectra of Series-B arrays can be blue shifted ($\Delta\lambda_{blue-shift}$) to a maximum of ~40.6 nm when the period was decreased from 500 to 200 nm as shown in Fig. 6(a). The magnitude of blue shift is in direct proportion to the estimated refractive index of the P3HT/PMMA square hole array (Fig. 6(b and c)). The geometrical parameters of the P3HT/PMMA medium arrays (i.e. period (L), hole diameter (D_{hole}) and hole area ratio), their estimated refractive indexes, the wavelengths of extinction peak (λ_{max}) and the blue shifts ($\Delta\lambda_{blue-shift}$) of extinction peak are summarized in Table 1. The slope of blue shift ($\Delta\lambda_{blue-shift}$) versus estimated refractive index of Series-B arrays (Fig. 6(c)) is larger than that of Series-A arrays (Fig. 3(c)) which indicates a stronger coupling effect occurred in Series-B arrays. This means that changing the periods of P3HT/PMMA square hole arrays with a fixed 100 nm hole results in a better tunability of the extinction spectra. From the above data,

Table 1
Geometrical parameters and characteristics of extinction spectra of P3HT/PMMA medium square hole arrays.

Samples	L (nm)	D_{hole} (nm)	Hole area ratio (%)	Estimated refractive index	λ_{max} (nm)	$\Delta\lambda_{blue-shift} = \|.\lambda_{max} - \lambda_0\|.$ (nm)
Thin film	–	–	–	$n_{P3HT/PMMA} = 1.50$	$\lambda_0 = 457.8$	–
A1	500	100	3.1	1.49	446.9	10.9
A2	500	220	15.2	1.43	444.6	13.2
A3	500	260	21.2	1.40	443.8	14.0
A4	500	320	32.2	1.34	434.8	23.0
A5	500	390	47.8	1.26	430.2	27.6
B1	200	100	19.6	1.40	417.2	40.6
B2	300	100	8.7	1.46	432.6	25.2
B3	400	100	4.9	1.48	444.8	13.0
B4	500	100	3.1	1.49	446.9	10.9

we can derive an equation that can predict the magnitude of blue shift of extinction spectra of P3HT/PMMA medium array as the following.

$$\Delta\lambda_{blue-shift} = \kappa \cdot \Delta n_{medium} \cdot c \tag{1}$$

In this equation, we assumed that κ is a constant including the characteristics of gold nanoparticle size and interparticle distance. The value of κ is fixed in this study, because we were using the same type of self-assembled gold nanoparticles on the silicon substrate. Δn_{medium} is the differences of estimated refractive index of P3HT/PMMA medium with different array structure, and c is an array structure factor that results from the changes of array structure, such as c_A is for Series-A arrays and c_B is for Series-B arrays. Comparing the two arrays, c_B is 4.1 times larger than c_A obtained from the slope of linear fitting (Fig.s 3(c) and 6(c)). Therefore, changing the period of medium array with a fixed hole diameter (Series-B arrays) is more effective for tuning the P3HT/PMMA extinction spectra than changing the hole diameter of medium array with a fixed period (Series-A arrays). Jain and El-Sayed reported that the increase in the medium dielectric constant for each metal particle results in a reduction in the Coulombic restoring force acting on the polarized electrons, and it means an increase in the electric dipole moment. Hence, the SPR coupling-induced red shift resulting from the electromagnetic coupling between noble metal nanoparticles increases with an increase in the dielectric constant of the medium [30]. Our experimental results and FDTD simulations show the blue shift as the dielectric constant of the medium decreases, which are consistent with their study.
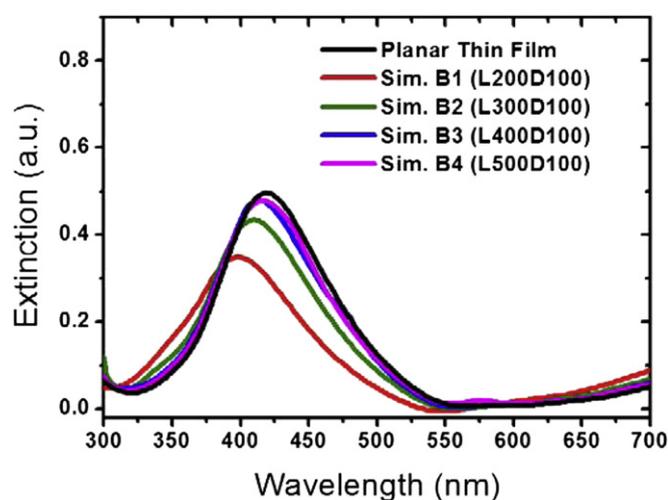
Fig. 7. Simulated extinction spectra of Series-B arrays have a fixed hole diameter of 100 nm with different periods (200, 300, 400 and 500 nm).

In contrast, the FDTD simulation of Series-B arrays as shown in Fig. 7 is similar to the experimental data as shown in Fig. 6(a). The extinction peak shift and decayed intensity magnitude are comparable. For example, the experimental data of B1-array shows an extinction peak blue shift of 40.6 nm and a decayed intensity of 28.2%, and the simulation results of B1-array shows about 21.5 nm for extinction peak blue shift and the decay of 23.6% for intensity. Although blue shift scales have some fractional errors, the trends of peak shift and intensity decays have good congruence. The difference between our experimental results and simulations may be due to complications such as P3HT absorption characteristics, the light illumination angles, several plasmon resonance modes with different polarization behaviors, and spectral overlap between different modes resulting in an extremely broad plasmon band [30,38,39].

4. Conclusions

In this study, we have established a simple method for tuning the extinction spectra of P3HT/PMMA by altering the medium arrays on self-assembled gold nanoparticles coated silicon substrate. The medium effect is observed due to the extent of coupling between P3HT/PMMA absorption and gold nanoparticle SPR is varied with the changing of P3HT/PMMA medium array. The magnitude of blue shift of the extinction spectra of P3HT/PMMA medium arrays is directly proportional to the product of the difference of medium refractive index and the array structure factor. We observed that the effects of near-field coupling can blue shift the extinction peak of $\sim$40.6 nm by varying the period of P3HT/PMMA medium square arrays with a fixed hole diameter of 100 nm. By comparison to FDTD simulation, the dependence of peak shift and intensity of extinction spectra on medium arrays alteration can be well described. The extinction peak is mainly from the absorption characteristics of the P3HT/PMMA, and adding the gold nanoparticles can give more functionalities for sensing applications, such as SERS. This new technology to control the extinction spectra of the medium by varying the medium arrays on gold nanoparticles surface plasmon resonance will open many opportunities for the design and fabrication of new optoelectronic devices and sensors.

Acknowledgment

carried out using the Elionix facility located in the Center for Information and Electronics Technologies of National Taiwan University.

Appendix A. Supplementary data

Supplementary data related to this article can be found at http://dx.doi.org/10.1016/j.matchemphys.2012.08.020.

References

[1] D. Langheinrich, E. Yslas, M. Broglia, V. Rivarola, D. Acevedo, A. Lasagni, Polym. Phys. 50 (2012) 415.
[2] G. Böttger, C. Liguda, M. Schmidt, M. Eich, Appl. Phys. Lett. 81 (2002) 2517.
[3] C.-S. Wu, C.-F. Lin, H.-Y. Lin, C.-L. Lee, C.-D. Chen, Adv. Mater. 19 (2007) 3052.
[4] D.-H. Ko, J.R. Tumbleston, A. Gadisa, M. Aryal, Y. Liu, R. Lopez, E.T. Samulski, J. Mater. Chem. 21 (2011) 16293.
[5] A.J. Haes, R.P. Van Duyne, J. Am. Chem. Soc. 124 (2002) 10596.
[6] T. Rindzevicius, Y. Alaverdyan, M. Käll, W.A. Murray, W.L. Barnes, J. Phys. Chem. C 111 (2007) 11806.
[7] M.W. Tsai, T.H. Chuang, H.Y. Chang, S.C. Lee, Appl. Phys. Lett. 88 (2006) 213112.
[8] P. Hanarp, M. Käll, D.S. Sutherland, J. Phys. Chem. B 107 (2003) 5768.
[9] M.C. Wu, Y. Chou, C.M. Chuang, C.P. Hsu, C.F. Lin, Y.F. Chen, W.F. Su, ACS Appl. Mater. Interf. 1 (2009) 2484.
[10] J.H. Song, T. Atay, S. Shi, H. Urabe, A.V. Nurmikko, Nano Lett. 5 (2005) 1557.
[11] M.C. Wu, C.M. Chuang, H.H. Lo, K.C. Cheng, Y.F. Chen, W.F. Su, Thin Solid Films 517 (2008) 863.
[12] O. Dong, D.C.C. Lam, Mater. Chem. Phys. 126 (2011) 91.
[13] W.L. Barnes, A. Dereux, T.W. Ebbesen, Nature 424 (2003) 824.
[14] H. Ko, S. Singamaneni, V.V. Tsukruk, Small 4 (2008) 1576.
[15] P. Cheng, D. Li, Z. Yuan, P. Chen, D. Yang, Appl. Phys. Lett. 92 (2008) 041119.
[16] C.M. Chuang, M.C. Wu, W.F. Su, K.C. Cheng, Y.F. Chen, Appl. Phys. Lett. 89 (2006) 061912.
[17] M.A. García, V. Bouzas, N. Carmona, Mater. Chem. Phys. 127 (2011) 446.
[18] C.F. Chen, S.D. Tzeng, H.Y. Chen, K.J. Lin, S. Gwo, J. Am. Chem. Soc. 130 (2008) 824.
[19] J. Prikulis, P. Hanarp, L. Olofsson, D. Sutherland, M. Käll, Nano Lett. 4 (2004) 1003.
[20] K. Okamoto, I. Niki, A. Shvartser, Y. Narukawa, T. Mukai, A. Scherer, Nat. Mater. 3 (2004) 601.
[21] T.H. Park, N. Mirin, J.B. Lassiter, C.L. Nehl, N.J. Halas, P. Nordlander, ACS Nano 2 (2008) 25.
[22] H. Wang, C.S. Levin, N.J. Halas, J. Am. Chem. Soc. 127 (2005) 14992.
[23] G. Laurent, N. Félidj, S.L. Truong, J. Aubard, G. Lévi, J.R. Krenn, A. Hohenau, A. Leitner, F.R. Aussenegg, Nano Lett. 5 (2005) 253.
[24] T.R. Jensen, M.L. Duval, K.L. Kelly, A.A. Lazarides, G.C. Schatz, R.P. Van Duyne, J. Phys. Chem. B 103 (1999) 9846.
[25] P.K. Jain, W. Qian, M.A. El-Sayed, J. Am. Chem. Soc. 128 (2006) 2426.
[26] J. Zhu, Y. Wang, L. Huang, Mater. Chem. Phys. 93 (2005) 383.
[27] S. Link, D.J. Hathcock, B. Nikoobakht, M.A. El-Sayed, Adv. Mater. 15 (2003) 393.
[28] A.J. Haes, W.P. Hall, L. Chang, W.L. Klein, R.P. Van Duyne, Nano Lett. 4 (2004) 1029.
[29] A.J. Haes, S. Zou, G.C. Schatz, R.P. Van Duyne, J. Phys. Chem. B 108 (2004) 6961.
[30] P.K. Jain, M.A. El-Sayed, Nano Lett. 8 (2008) 4347.
[31] J. Turkevich, Gold Bull. 18 (1985) 86.
[32] C.F. Chen, S.D. Tzeng, M.H. Lin, S. Gwo, Langmuir 22 (2006) 7819.
[33] W. Cheng, S. Dong, E. Wang, Chem. Mater. 15 (2003) 2495.
[34] M.C. Wu, C.H. Chang, H.H. Lo, Y.S. Lin, C.W. Chen, W.C. Yen, Y.Y. Lin, Y.F. Chen, W.F. Su, J. Mater. Chem. 18 (2008) 4097.
[35] P.B. Johnson, R.W. Christy, Phys. Rev. B 6 (1972) 4370.
[36] E.D. Palik, Handbook of Optical Constants of Solids, Academic, New York, 1985.
[37] S.N. Kasarova, N.G. Sultanova, C.D. Ivanov, I.D. Nikolov, Opt. Mater. 29 (2007) 1481.
[38] M.C. Wu, H.C. Liao, W.C. Yen, C.M. Chuang, Y.Y. Lin, C.W. Chen, Y.F. Chen, W.F. Su, J. Phys. Chem. B 114 (2010) 10277.
[39] P.K. Jain, W. Huang, M.A. El-Sayed, Nano Lett. 7 (2007) 2080.